



Review

# Structural Biology Inspired Development of a Series of Human Peroxisome Proliferator-Activated Receptor Gamma (PPAR $\gamma$ ) Ligands: From Agonist to Antagonist

Hiroyuki Miyachi

Lead Exploration Unit, Drug Discovery Initiative, The University of Tokyo, 7-3-1 Hongo, Bunkyo-ku, Tokyo 113-0033, Japan; miyachi\_hiroyuki@mol.f.u-tokyo.ac.jp

**Abstract:** Recent progress in the structural and molecular pharmacological understanding of the nuclear receptor, peroxisome proliferator-activated receptor gamma (hPPAR $\gamma$ )—a transcription factor with pleiotropic effects on biological responses—has enabled the investigation of various graded hPPAR $\gamma$  ligands (full agonist, partial agonist, and antagonist). Such ligands are useful tools to investigate the functions of hPPAR $\gamma$  in detail and are also candidate drugs for the treatment of hPPAR $\gamma$ -mediated diseases, such as metabolic syndrome and cancer. This review summarizes our medicinal chemistry research on the design, synthesis, and pharmacological evaluation of a covalent-binding and non-covalent-binding hPPAR $\gamma$  antagonist, both of which have been created based on our working hypothesis of the helix 12 (H12) holding induction/inhibition concept. X-ray crystallographic analyses of our representative antagonists complexed with an hPPAR $\gamma$  ligand binding domain (LBD) indicated the unique binding modes of hPPAR $\gamma$  LBD, which are quite different from the binding modes observed for hPPAR $\gamma$  agonists and partial agonists.

**Keywords:** peroxisome proliferator-activated receptor gamma; PPAR $\gamma$ ; antagonist; structural biology; ligand superfamily concept



**Citation:** Miyachi, H. Structural Biology Inspired Development of a Series of Human Peroxisome Proliferator-Activated Receptor Gamma (PPAR $\gamma$ ) Ligands: From Agonist to Antagonist. *Int. J. Mol. Sci.* **2023**, *24*, 3940. <https://doi.org/10.3390/ijms24043940>

Academic Editor:  
Anastasios Lymperopoulos

Received: 21 January 2023  
Revised: 11 February 2023  
Accepted: 12 February 2023  
Published: 15 February 2023



**Copyright:** © 2023 by the author. Licensee MDPI, Basel, Switzerland. This article is an open access article distributed under the terms and conditions of the Creative Commons Attribution (CC BY) license (<https://creativecommons.org/licenses/by/4.0/>).

## 1. Peroxisome Proliferator-Activated Receptor Gamma (PPAR $\gamma$ )

Human peroxisome proliferator-activated receptors (hPPARs) are ligand-mediated transcription factors belonging to the human 48 nuclear receptor (NR) superfamily, which includes the retinoid receptor, steroid receptor, vitamin D receptor, and others [1]. Three subtypes of hPPARs—hPPAR $\alpha$  [NR1C1], hPPAR $\delta$  [NR1C2], and hPPAR $\gamma$  [NR1C3]—have been identified to date in various species, including humans [2]. Upon endogenous and/or exogenous agonist binding, hPPARs heterodimerize with another nuclear receptor—the retinoid X receptor—in the nucleus and these heterodimers regulate gene expression by binding to the specific consensus DNA sequences, termed peroxisome proliferator responsive elements (PPREs) in the promoter regions of the target genes. The structural basis of PPREs is a direct repeat of the hexameric AGGTCA recognition motif, separated by one nucleotide (termed DR1) [3].

The hPPARs have five conserved structural domains: A–E domains from the N- to C-terminus [4]. The N-terminal A and B domains contain activation function 1 (AF1), which is involved in ligand-independent coregulator binding. The C domain functions as a DNA binding domain and is the most conserved domain among the hPPARs. The D domain functions as a flexible hinge allowing rotation between the DNA binding domain (C domain) and ligand binding domain (E domain), as well as containing a nuclear localization signal. The E domain is the largest domain in hPPARs and is the second most conserved domain among the hPPARs. There are four main functions of the E domain: it is a second dimerization interface, a ligand binding pocket, and a coregulator binding surface, and activation function 2 (AF2) acts as a binding site for coregulator proteins.

The hPPAR $\gamma$  is mainly expressed in adipose tissue, macrophages, vascular smooth muscle, and in tumors originating from various organs [5]. An early study reported hPPAR $\gamma$  had a key role in regulating adipocyte differentiation [6] and insulin sensitivity [7]. Therefore, modulators of hPPAR $\gamma$  activity have the potential for the treatment of type 2 diabetes. hPPAR $\gamma$  full agonists—glitazone class drugs (TZD) such as pioglitazone and rosiglitazone—are used for the treatment of type 2 diabetes [8]. Despite the beneficial clinical effects of these drugs, TZDs cause several adverse effects, including significant weight gain, peripheral edema, bone loss, and an increased risk of congestive heart failure, mainly arising from their over-activation of hPPAR $\gamma$  [9]. Thus, novel hPPAR $\gamma$ -modulating agents that activate hPPAR $\gamma$  moderately, not fully, clearly need to be developed. Phosphorylation of Ser245 of hPPAR $\gamma$  with cyclin-dependent kinase 5 (Cdk5) is an important post-translational modification of hPPAR $\gamma$  [10]. CDK5 does not alter its adipogenic activity but dysregulated a specific set of genes with important roles in obesity and diabetes. Recently, an hPPAR $\gamma$  antagonist was reported to block hPPAR $\gamma$  phosphorylation and exert anti-diabetic activity with fewer side effects compared with the hPPAR $\gamma$  full agonist by its direct binding to a site near the  $\beta$ -sheet and helix H3 of hPPAR $\gamma$  [11], which was recently shown to be an alternate/allosteric binding site [12].

From a historical point of view, the hPPAR $\gamma$  ligand discovery program was initially focused on the identification of hPPAR $\gamma$  full and partial agonists. Later, molecular pharmacology research indicated the significance of antagonist-mediated hPPAR $\gamma$  signal transduction for drug discovery.

This evidence demonstrates that hPPAR $\gamma$  agonists and antagonists are attractive molecular targets for the treatment of various diseases, including not only type II diabetes and cancer, but also new targets, such as epilepsy [13], allergies [14], and non-alcoholic fatty liver disease (NAFLD) [15]. Therefore, potent hPPAR $\gamma$ -selective ligands should be developed. Previously, we summarized our structural development studies in historical order to create hPPAR subtype-selective agonists [16]. The discovery of many types of hPPAR ligands indicates the validity of our strategy to create subtype-selective hPPAR agonists. In this review, we summarize our structural development studies to create covalent-binding and non-covalent-binding hPPAR $\gamma$  antagonists.

## 2. Working Hypothesis to Create a PPAR $\gamma$ Antagonist from PPAR $\gamma$ Agonist 1

Previously, we reported that nuclear receptor antagonists can be designed and synthesized in accordance with the helix 12 (H12) proper folding inhibition hypothesis [17]. This hypothesis was created based on the results of a number of X-ray crystallographic analyses of NR ligand binding domains (LBDs) with or without a bound agonist, focusing on the agonist-induced proper folding of the H12 of NR LBDs. In the absence of an agonist, H12 exists in various open conformations, which might be favorable for the recruitment of corepressors that induce the transrepression of the NR signal transduction. However, once a full agonist binds to the ligand-binding pocket (LBP) of the NR—forming a hydrogen bond network with the receptor—H12 forms a closed, solvent-exposed active conformation, which consequently stabilizes the AF-2 region of the NR. This stabilization facilitates the dissociation of the corepressor followed by the association of a coactivator with the receptor to induce its transactivation. Thus, an agonist that induces the proper folding of H12 might be required to initiate the transcriptional processes. On the basis of these considerations, ligands that bind to the LBP and interfere with the proper folding of H12 should be antagonists of the corresponding NR. In accordance with this hypothesis, we successfully designed and synthesized a range of NR antagonists, including retinoic acid receptor antagonists [18], liver X receptor antagonists [19], and farnesoid X receptor antagonists [20].

To create structurally new hPPAR $\gamma$  antagonists based on this working hypothesis, we initially focused on our previously created hPPAR $\gamma$ -selective agonist MEKT-21 ( $EC_{50} = 0.08 \pm 0.009 \mu\text{M}$ ,  $E_{\text{max}} = 80 \pm 3.1\%$  relative to the hPPAR $\gamma$  pan agonist, TIPP-703, in our assay system) as a template [21] because we solved its X-ray crystal structure com-

plexed with hPPAR $\gamma$  LBD. From the complex structure, we noted that the flexible  $\alpha$ -ethyl phenylpropanoic acid moiety formed a hydrogen bond network with the side chain amino acids of Ser289, His323, Tyr327, and Tyr473 of the hPPAR $\gamma$  LBD. Of these, the hydrogen bond interaction between the carboxylic acid moiety of TIPP-703 with Tyr473 on H12 was critically important for the proper folding of the H12 of the hPPAR $\gamma$  and the transactivation of the target genes [22]. Therefore, an effective approach for antagonist design should be the disruption of this key interaction by the replacement of the carboxyl group of MEKT-21 with other functional groups, such as an acylsulfonamide group (plan A in Figure 1) to obtain two important derivatives: a phenyl sulfonyl amino carbonyl derivative (MEKT-75 (7a)) and a benzyl sulfonyl amino carbonyl derivative (MEKT-76 (7b)).

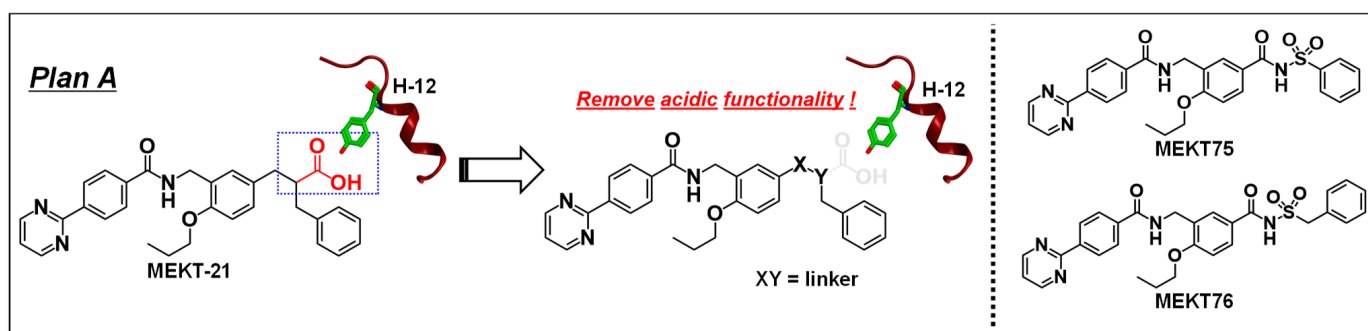
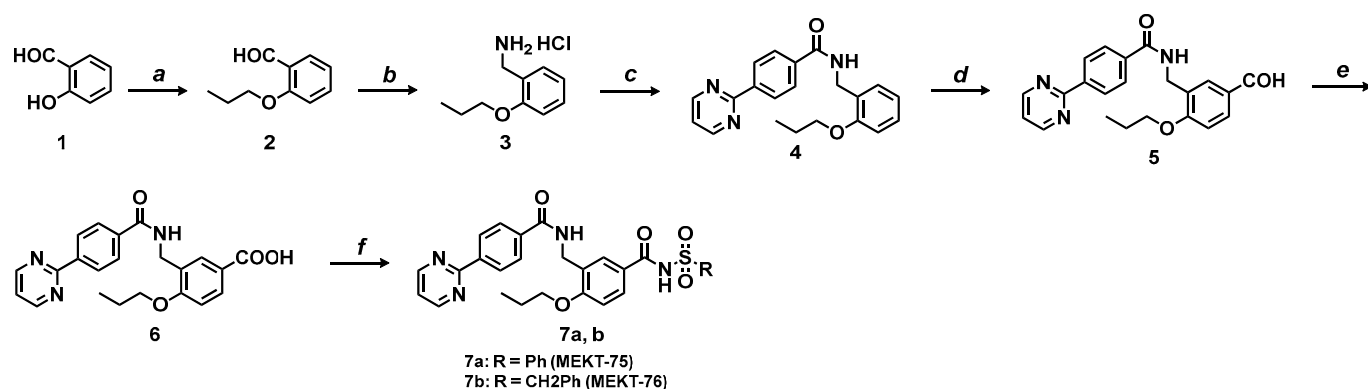


**Figure 1.** The strategic plan A to create hPPAR $\gamma$  antagonists.

The synthetic production of MEKT-75 and MEKT-76 is shown in Scheme 1. Salicylaldehyde **1** was alkylated with *n*-propyl iodide to give salicylaldehyde **2**. Compound **2** was amide alkylated with *t*-butyl carbamate followed by acid hydrolysis to afford aminomethylbenzene derivative **3** as a hydrochloric acid salt. Compound **3** was condensed with 4-(2-pyrimidinyl)benzoic acid in the presence of DEPC and resulting product **4** was regioselectively formylated (**5**), followed by Pinnick oxidation to afford benzoic acid **6**. Compound **6** was condensed with benzenesulfonamide (or benzyl sulfonamide) in the presence of EDC and DMAP to afford the target compounds MEKT-75 and MEKT-76.



**Scheme 1.** The synthetic production of MEKT-75 and MEKT-76. **Reagents and conditions:** (a) *n*-PrI, K<sub>2</sub>CO<sub>3</sub>, DMF, 80 °C, 24 h, 89%. (b) (1) *t*BuOOC-NH<sub>2</sub>, TFA, Et<sub>3</sub>SiH, r.t., 12 h. (2) (2) 4M HCl, AcOEt, r.t., 2.5h, 89% (2 steps). (c) Pyrimidine-2-ylbenzoic acid, DEPC, TEA, DMF, r.t., overnight, 64%. (d) TiCl<sub>4</sub>, CH<sub>3</sub>OCHCl<sub>2</sub>, DCM, 0 °C to r.t., overnight, 71%. (e) NaClO<sub>2</sub>, NaH<sub>2</sub>PO<sub>4</sub>·2H<sub>2</sub>O, 2-methyl-2-butene, *t*-BuOH/THF/H<sub>2</sub>O, r.t., overnight, 90%. (f) Benzene (or benzyl) sulfonamide, EDC, DMAP, DMF, r.t., overnight, 27–30%.

We evaluated the transactivation activities of MEKT-75 and MEKT-76 (Figure 2 left). MEKT-75 exhibited significant transactivation activity; however, dose-dependency was not seen and it reached about 50% of the maximal activity obtained from the maximal response

of the positive control (10  $\mu$ M pioglitazone (hPPAR $\gamma$  full agonist)) at the concentration of 10  $\mu$ M. These experimental results clearly indicated that MEKT-75 is an hPPAR $\gamma$  partial agonist [23].

MEKT-76 exhibited lower transactivation activity compared with the positive control; about 40% of the maximal activity obtained from the maximal response of the positive control at the highest concentration of 30  $\mu$ M. Of note, MEKT-76 dose-dependently inhibited the transactivation activity elicited by 10  $\mu$ M of the hPPAR $\gamma$  full agonist, pioglitazone (Figure 2 right). These data indicate that MEKT-76 is a far less potent hPPAR $\gamma$  partial agonist than MEKT-75 and is weak enough to exhibit an antagonistic nature when co-treated with an hPPAR $\gamma$  full agonist [24].

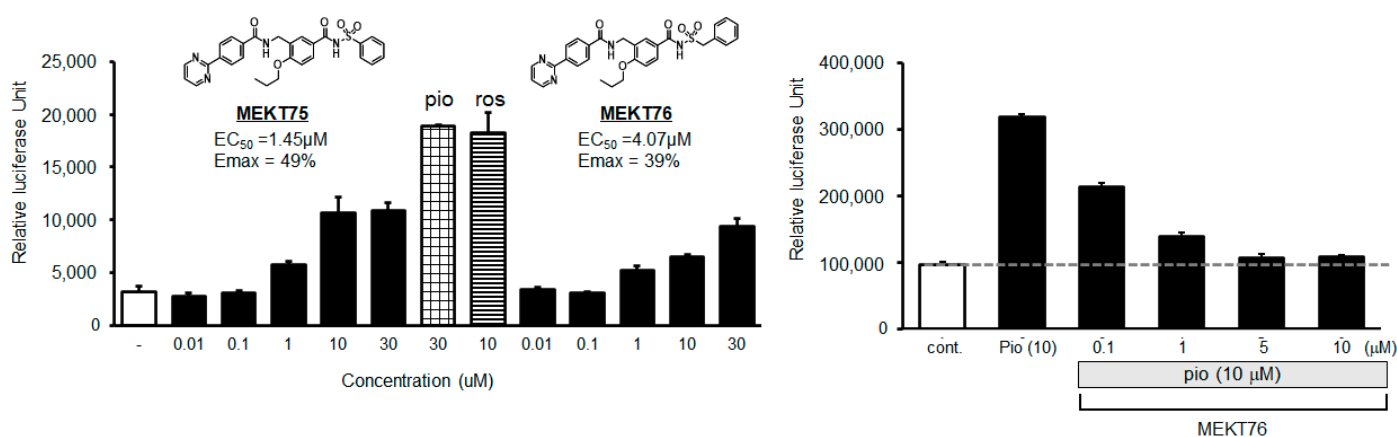


**Figure 2.** The transactivation and transrepression activities elicited by MEKT-75 and MEKT-76. (Left) Dose–response relationships of the hPPAR $\gamma$  agonistic activities of MEKT-75 and MEKT-76. pio: pioglitazone. ros: rosiglitazone (hPPAR $\gamma$  full agonists). (Right) Dose–response relationships for the hPPAR $\gamma$  antagonistic activity of MEKT-76 in the presence of 10  $\mu$ M pioglitazone.

To understand the substantial differences between the transactivation/transrepression activities of these two derivatives, we solved their X-ray crystal structures complexed with the hPPAR $\gamma$  LBD at resolutions of 2.1  $\text{\AA}$  and 2.2  $\text{\AA}$ , respectively. A crystal of the complex was obtained by soaking a crystal of the homodimer in ligand solution. The results are summarized in Figure 3.

The hPPAR $\gamma$  LBD–MEKT-75 crystal formed a homodimer and each hPPAR $\gamma$  LBD bound to one molecule of MEKT-75 (Figure 3A). It is important to note that each structural fold of hPPAR $\gamma$  LBD was similar except from the end of helix 11 (H11) to the C-terminal H12 region. Two bound ligands in each hPPAR $\gamma$  LBD–MEKT-75 complex had a similar three-dimensional structure and were situated in arm2 and arm3 of the binding pocket of the hPPAR $\gamma$  LBD. One of the structural folds in the homodimer was similar to that obtained from the hPPAR $\gamma$  LBD–rosiglitazone (hPPAR $\gamma$  full-agonist) complex (Figure 3A,B) [25]. Therefore, we tentatively designated the former structure as the fully active form of the PPAR $\gamma$  LBD and the latter structure as a non-fully active form.

In the fully active form, MEKT-75 has a U-shaped structure and the acylsulfonamide group of MEKT-75 is positioned near H11. Interactions of three of the five key amino acids (Ser289, His323, Tyr327, His449, and Tyr473), which are critical for the construction of hydrogen bond networks, were conserved in the one LBD complexed with MEKT-75. This appeared to be sufficient to support the fully active LBD structure. In contrast, in the non-fully active form, another interaction was noted: His266 was located close to the (pyrimidin-2-yl)phenyl moiety of MEKT-75, resulting in a hydrophobic interaction between His266 and the phenyl group and between His266 and the pyrimidin-2-yl group. These additional interactions caused bound MEKT-75 to move to the right, so that the distance from the phenyl sulfonyl amino carbonyl group of MEKT-75 to the side chains of the surrounding amino acids became longer. As a result, the hydrogen bond network was

weaker, suggesting that the H12 region is not restricted to the appropriate location for full activity.

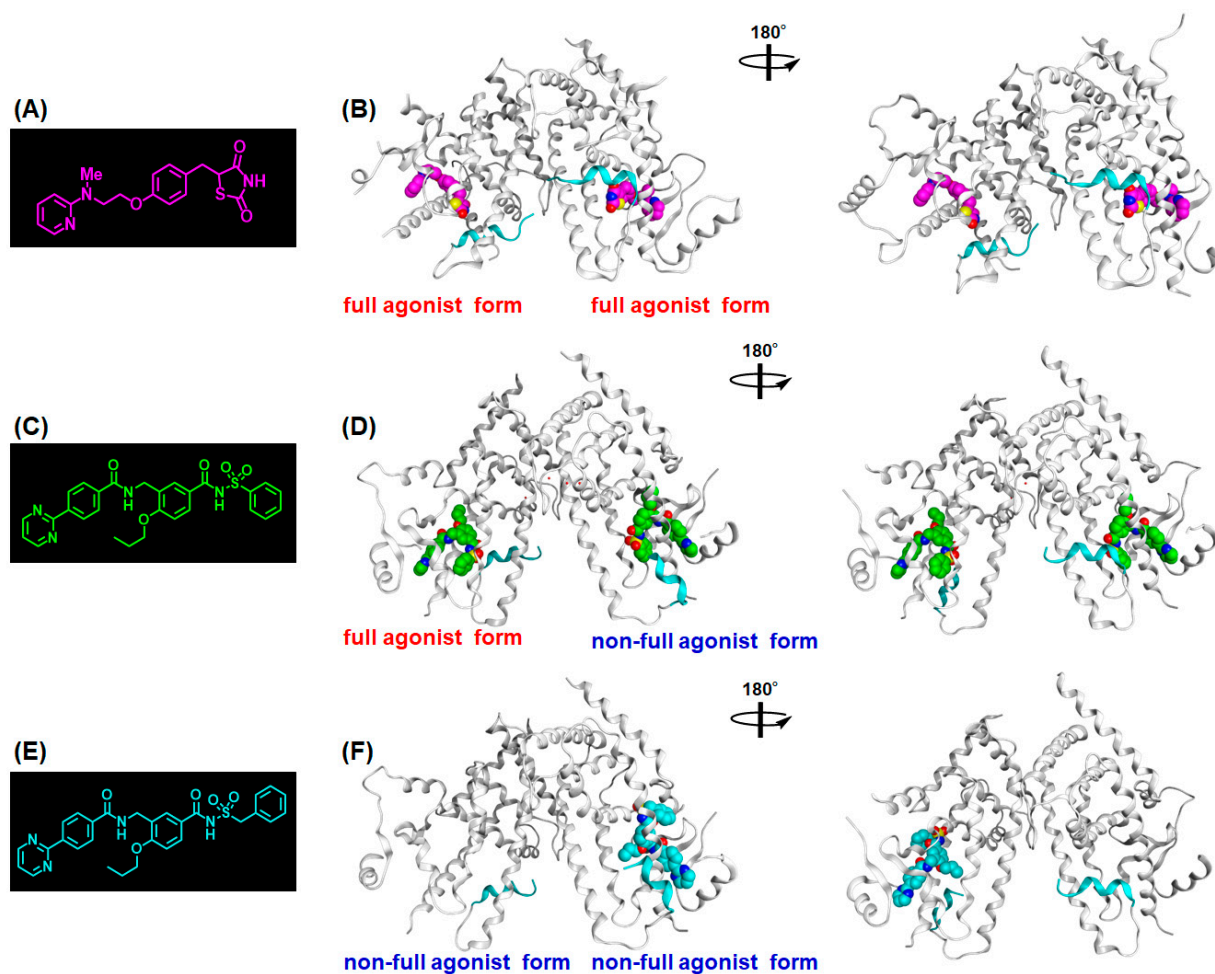


**Figure 3.** A comparison of the hPPAR $\gamma$  ligands complexed with the hPPAR $\gamma$  LBD. (A) Chemical structure of rosiglitazone. (B) Whole structure of the hPPAR $\gamma$  LBD–rosiglitazone homodimer (PDB: 2PRG). Proteins are represented as a gray ribbon model and rosiglitazone is depicted as a magenta van der Waals model. (C) Chemical structure of MEKT-75. (D) Whole structure of the hPPAR $\gamma$  LBD–MEKT-75 homodimer (PDB:3WMH). Proteins are represented as a gray ribbon model and MEKT-75 is depicted as a green van der Waals model. (E) Chemical structure of MEKT-76. (F) Whole structure of the hPPAR $\gamma$  LBD–MEKT-76 homodimer (PDB:4YT1). Proteins are represented as a gray van der Waals surface model and MEKT-76 is depicted as a cyan van der Waals model.

The hPPAR $\gamma$  LBD–rosiglitazone complex also formed a homodimer in its crystal form, but each LBD was present in its fully active form (Figure 3B). This result indicated that the full agonist induced a conformational change of the non-fully active hPPAR $\gamma$  LBD to the fully active LBD, presumably by facilitating a tight hydrogen bond network with the LBD.

The hPPAR $\gamma$  LBD–MEKT-76 crystal also formed a homodimer, but only one molecule of MEKT-76 was bound to the hPPAR $\gamma$  LBD. The structural fold of the bound hPPAR $\gamma$  LBD was similar to that of the non-fully active form of the LBD complexed with MEKT-75. The 4-(pyrimidin-2-yl)benzamide side chain of MEKT-76 was docked into a large pocket composed of H2,  $\beta$ 2, H3, and H5, which made hydrophobic contact with the surrounding amino acid residues. The benzyl sulfonyl amino carbonyl side chain was docked between the side chains of the amino acids of H3 and H5, which made hydrophobic contact with the surrounding amino acid residues. The *n*-propoxy side chain of MEKT-76 was located between the side chains of the amino acids of H6 and H7 and H11. Only His449—a key

amino acid (Ser289, His323, Tyr327, His449, and Tyr473) for hPPAR $\gamma$ -agonistic activity—contributed to the formation of the hydrogen bond interactions. Therefore, the present X-ray structure is consistent with the idea that MEKT-76 is a very weak hPPAR $\gamma$  partial agonist, because both hPPAR $\gamma$  LBDs in the homodimeric complex had a non-fully active structure and MEKT-76 was loosely bound in the binding pocket of only one of the homodimer complexes.

The rank order of the interaction energy between rosiglitazone, MEKT-75, and MEKT-76 correlated with the hPPAR $\gamma$  agonistic nature. Figure 4 shows the binding energy results of rosiglitazone, MEKT-75, and MEKT-76. The total interaction energy of rosiglitazone (hPPAR $\gamma$  full agonist) to the full agonist form of the hPPAR $\gamma$  LBD was  $-125.24$  kcal/mol (calculated using the van der Waals (vdW) interaction energy ( $-43.68$  kcal/mol) and electrostatic (ele) interaction energy ( $-81.56$  kcal/mol); the relative vdW interaction energy (vdW/volume) was  $-0.14$  kcal/mol and the relative ele interaction energy (ele/volume) was  $-0.25$  kcal/mol) [26]. This indicated that rosiglitazone was docked into the full agonist form of hPPAR $\gamma$  LBD primarily with electrostatic interactions. For the MEKT-75 full agonist form of the hPPAR $\gamma$  LBD, the total interaction energy of MEKT-75 to the full agonist form of the hPPAR $\gamma$  LBD was  $-137.65$  kcal/mol (calculated using the vdW interaction energy ( $-78.95$  kcal/mol) and ele interaction energy ( $-58.70$  kcal/mol)—the relative vdW interaction energy (vdW/volume) was  $-0.17$  kcal/mol and the relative ele interaction energy (ele/volume) was  $-0.13$  kcal/mol). These data indicated that MEKT-75 was docked into the full agonist form of the hPPAR $\gamma$  LBD with comparable van der Waals interactions and electrostatic interactions. Although the relative vdW interaction energy was comparable to that of rosiglitazone, the relative ele interaction energy (ele/volume) was only one-half of that of rosiglitazone. This decreased relative ele interaction energy might contribute to the hPPAR $\gamma$  partial agonist nature of MEKT-75.

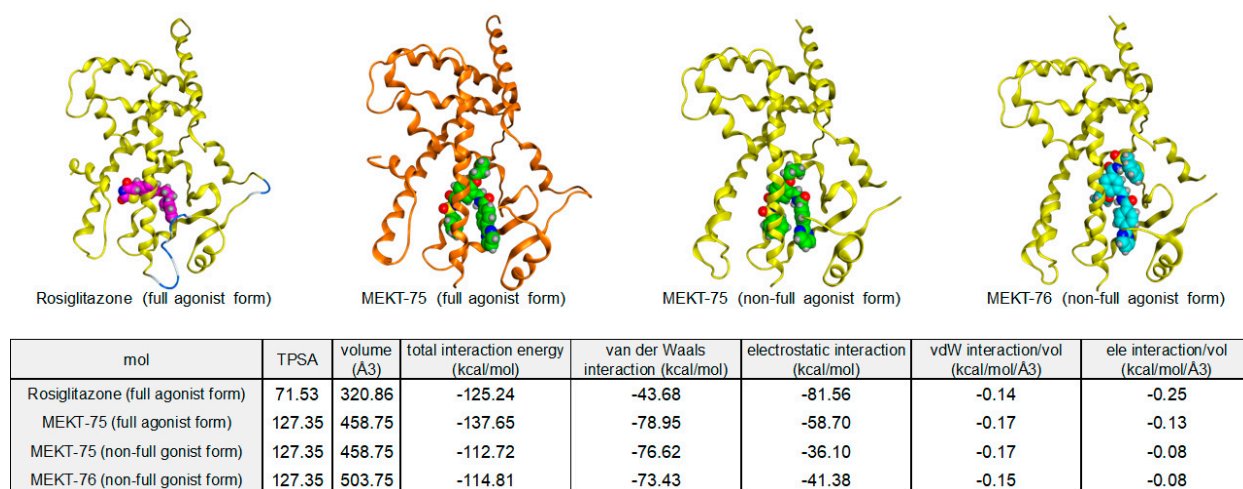


**Figure 4.** The binding energy comparison between hPPAR $\gamma$  ligands complexed with hPPAR $\gamma$  LBD. (Up) Monomeric structures of the hPPAR $\gamma$  LBD ligand. (Down) Summary of the binding energy calculations of rosiglitazone, MEKT-75, and MEKT-76 complexed with hPPAR $\gamma$  LBD.

For both non-full agonist forms of the hPPAR $\gamma$  LBD complexed with MEKT-75 and MEKT-76, the total interaction energy of the non-full agonist form of the hPPAR $\gamma$  LBD was about  $-114$  kcal/mol (calculated using the vdW interaction energy ( $-75$  kcal/mol) and ele interaction energy ( $-39$  kcal/mol); the relative vdW interaction energy (vdW/volume) was  $-0.16$  kcal/mol and the relative ele interaction energy (ele/volume) was  $-0.08$  kcal/mol). These data indicated that both compounds were docked into the non-full agonist form of the hPPAR $\gamma$  LBD primarily with van der Waals interactions.

Although MEKT-76 is only a homolog of MEKT-75, the binding mode of MEKT-76 complexed with the hPPAR $\gamma$  LBD was quite different from that obtained with MEKT-75. The bound parts of the benzyl sulfonyl amino carbonyl side chain and the *n*-propoxy

side chain of MEKT-76 were docked into the opposite binding pockets compared with the corresponding side chains of MEKT-75. Figure 5 shows the superimposed structures of bound MEKT-75 and bound MEKT-76 complexed with the hPPAR $\gamma$  LBD, and Figure 5B,E and Figure 5C,F show the binding modes of MEKT-75 and MEKT-76 complexed with the hPPAR $\gamma$  LBD, respectively. In Figure 5D, the hinge region benzene rings poorly overlap with each other. The hinge region benzene ring of MEKT-76 was shifted by a distance equivalent to one benzene ring compared with its position in MEKT-75. The most significant difference between the binding modes of both compounds was the position of the two substituents at the hinge region benzene ring. These substituents of MEKT-75 and MEKT-76 were in opposite directions (180° difference). For MEKT-75 complexed with the hPPAR $\gamma$  LBD, the phenyl sulfonyl amino carbonyl group faced Tyr327, which is a critically important amino acid for full agonistic activity and has hydrogen bonding interactions with the surrounding key amino acids. However, in the MEKT-76 complex, the benzyl sulfonyl amino carbonyl group was flipped in the other direction and the *n*-propoxy group faced Tyr327, but had no apparent hydrogen bond interactions with the surrounding key amino acids.

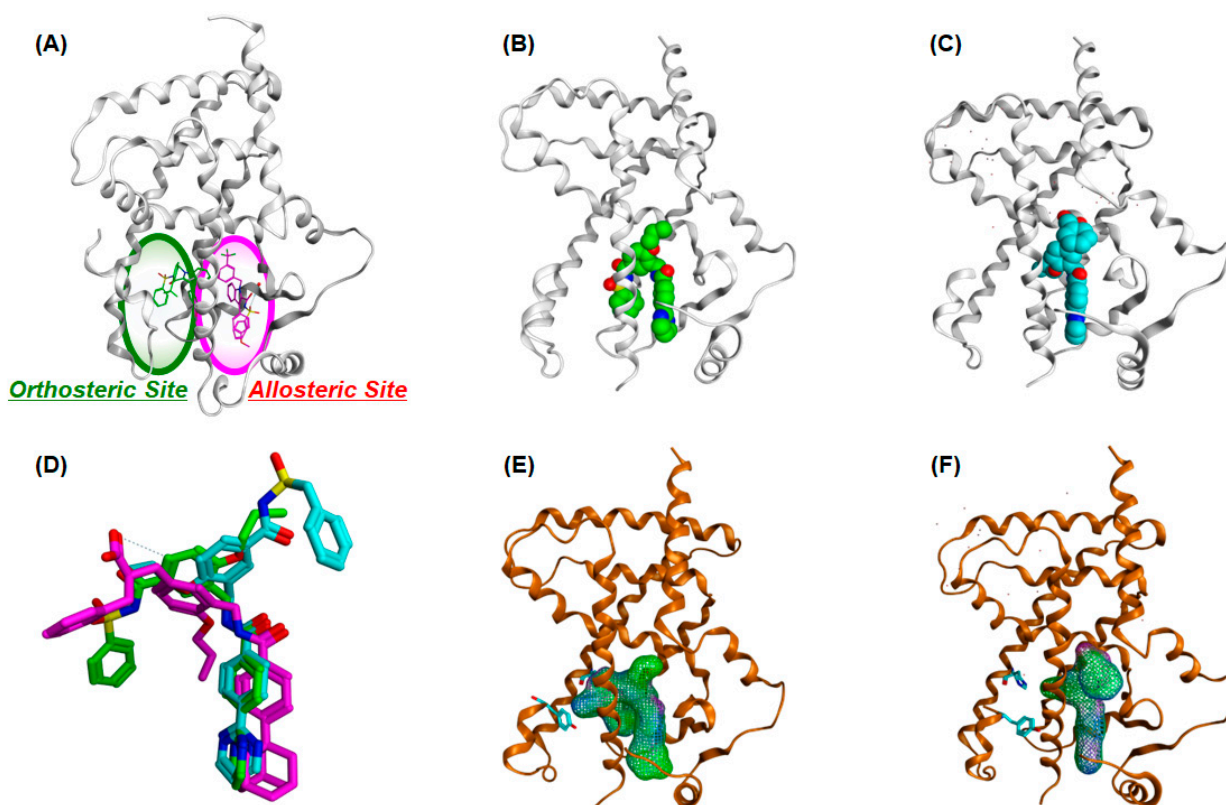


**Figure 5.** The binding mode differences between MEKT-75 and MEKT-76. (A) Co-crystal structure of NSI-bound hPPAR $\gamma$  (PDB 2HFP) shows two bound carboxamide molecules, one bound to the orthosteric site (green) and the second bound to the allosteric site (magenta). (B) Whole structure of the non-full agonist form of PPAR $\gamma$  LBD–MEKT-75. Proteins are represented as a van der Waals surface model and MEKT-75 is depicted as a green van der Waals model. (C) Whole structure of the non-full agonist form of PPAR $\gamma$  LBD–MEKT-76. Proteins are represented as a van der Waals surface model and MEKT-75 is depicted as a cyan van der Waals model. (D) Zoomed-in view of the entrance region of the PPAR $\gamma$  LBD–MMT-160 complex. (E) Whole structure of the non-full agonist form of PPAR $\gamma$  LBD–MEKT-75. Proteins are represented as a van der Waals surface model and the surface area of MEKT-75 is depicted. (F) Whole structure of the non-full agonist form of PPAR $\gamma$  LBD–MEKT-76. Proteins are represented as a van der Waals surface model and the surface area of MEKT-76 is depicted.

Recent structural biology studies indicated that the hPPAR $\gamma$  LBP can be divided into two regions. One is for the orthosteric binding pocket and the other is for the alternate (allosteric) binding pocket (Figure 5A) [27]. The orthosteric binding pocket is defined by helices 5, 7, and 11, whereas the alternate binding site consists of helices H2, H3, and  $\beta$ -sheets. The entrance to the ligand binding site of the hPPAR $\gamma$  LBD was reported to be between H3 and the three-stranded antiparallel  $\beta$ -sheets [28].

We thus speculated that the binding of MEKT-76 at the alternate (allosteric) binding pocket shielded the entrance site of the ligands, which might explain why MEKT-76 exhibited antagonistic activity when co-treated with an hPPAR $\gamma$  full agonist.

### 3. Working Hypothesis to Create a PPAR $\gamma$ Antagonist from PPAR $\gamma$ Agonist 2

Although MEKT-76 demonstrated hPPAR $\gamma$  antagonistic activity, it involved intrinsic hPPAR $\gamma$  agonistic activity to some extent. Therefore, a strategy to delete the acidic carboxylic acid functionality of the hPPAR $\gamma$  agonist (plan A) was not effective for developing a complete hPPAR $\gamma$  antagonist.

As described previously, the hydrogen bond interaction with Tyr473 on the H12 of the hPPAR $\gamma$  LBD was considered critical for the proper folding of the H12 of the hPPAR $\gamma$  LBD, which stabilized the water-accessible, closed conformation, fully active form of H12. Therefore, an effective approach for antagonist design must block this key interaction. However, the X-ray crystal structures of MEKT-75 complexed with the hPPAR $\gamma$  LBD indicated that although the acylsulfonamide group of MEKT-75 had no direct hydrogen bond interaction with Tyr473, it formed hydrogen bonds with the other side chain amino acids of Tyr327 and His449 around the H12. Consequently, the overall structural fold of the hPPAR $\gamma$  LBD–MEKT-75 complex—including the H12 position—was very similar to that of the complex obtained with the hPPAR $\gamma$  full agonist, rosiglitazone. A lack of interactions between MEKT-75 and Tyr473 might explain the partial agonist nature of MEKT-75 because it is unable to completely inhibit the proper folding of H12. On the basis of this, we speculated that a folding inhibition-type full antagonist of hPPAR $\gamma$  should have no direct hydrogen bond interactions with the Tyr473 of H12 and should push the H12 out of position. This design concept is illustrated in Figure 6, plan B.

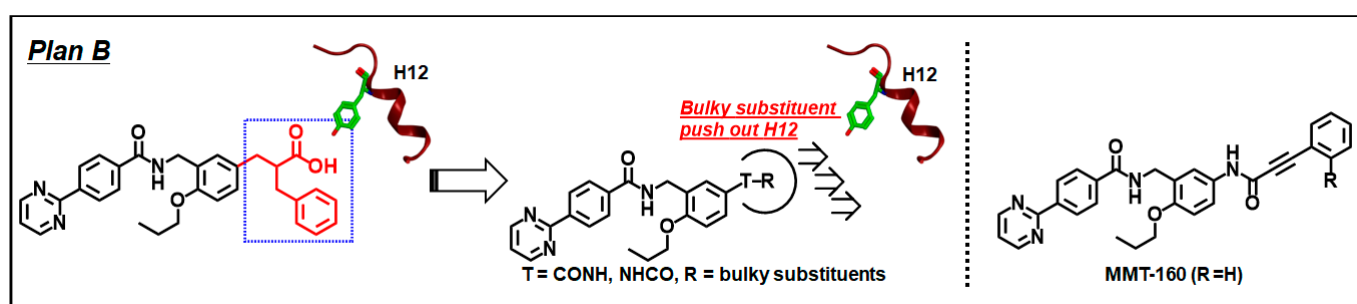
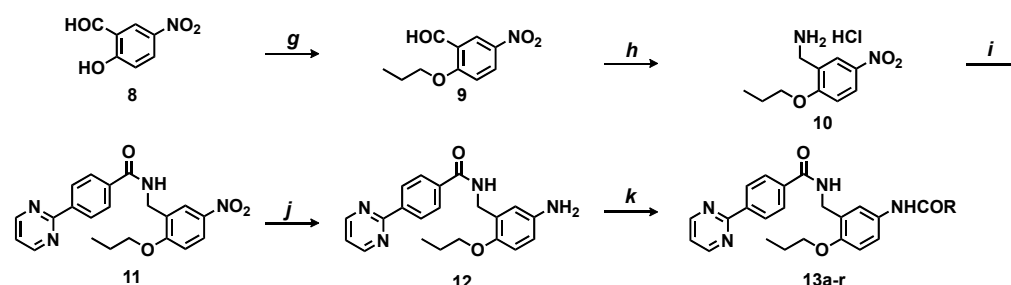


**Figure 6.** The strategic plan B to create hPPAR $\gamma$  antagonists.

Plan B contains two ideas. One is the removal of the acidic carboxyl group to disable hydrogen bond interactions with Tyr473, as in plan A. This is necessary to inhibit the full hPPAR $\gamma$  agonistic nature of the ligand. The other idea is the rigidification and expansion of the residual conformationally-flexible 3-phenylpropyl group of MEKT-21, which is expected to push the H12 out of the full agonist form position. Accordingly, we focused on a reversed amide linkage as the rigid tether, aiming to compensate for the loss of affinity caused by the deletion of the hydrogen bond interactions with Tyr473 [29].

The procedure to synthesize the reversed amide derivatives is depicted in Scheme 2. 5-nitrosalicylaldehyde (**8**) was *n*-propylated and then amide-alkylated with *t*-butylcarbamate in the presence of trifluoroacetic acid and triethylsilane [30], followed by the removal of the *N*-Boc protecting group to afford aminomethyl benzene derivative **10** as a hydrochloric acid salt. Compound **10** was condensed with 4-(2-pyrimidyl)benzoic acid and then the nitro

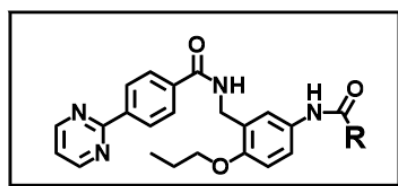
group was reduced to afford aniline **12**. Compound **12** was condensed with the appropriate carboxylic acid to afford the reversed amide derivatives **13a–r**.



**Scheme 2.** The synthesis of the reversed amide derivatives **13 a–r**. **Reagents and conditions:** (g) *n*-PrI,  $K_2CO_3$ , DMF, 80 °C, 24 h, 80%. (h) (1) *t*-BuOCONH<sub>2</sub>, TFA, Et<sub>3</sub>SiH, MeCN, r.t., 24 h. (2) 4 mol/L HCl in AcOEt, r.t., 3 h, 90% (2 steps). (i) 4-(pyrimidine-2-yl)benzoic acid, DEPC, TEA, dry DMF, r.t., overnight, 88%. (j) H<sub>2</sub>, 10%Pd/C, MeOH/AcOEt, r.t., 3 h, 98%. (k) carboxylic acids, HATU, DIEA, DMF, r.t., overnight, 25–44%.

As expected, the initial synthesized phenyl (**13a**), benzyl (**13b**), and 2-phenylethyl (**13c**) derivatives exhibited decreased hPPAR $\gamma$  agonistic activity compared with MEKT-21 (Figure 7), which might be related to the deletion of the acidic carboxyl group. Compounds **13a** and **13b** showed hPPAR $\gamma$  partial agonistic activities with moderate potency and low efficacy compared with the lead compound, MEKT-21. The increase in efficacy was in the order of phenyl < benzyl < 2-phenethyl derivatives. These results prompted us to speculate that the substituents bearing single bonds such as the benzyl or 2-phenethyl group did not efficiently push H12 out of position because of its conformational flexibility. Of these compounds, **13a** was the most potent hPPAR $\gamma$  partial agonist with low efficacy; therefore, we focused on **13a** as the next lead compound and prepared **13a** derivatives. The introduction of more rigid and bulkier substituents such as 4-ethynylphenyl (**13d**), 1-naphthyl (**13e**), 2-naphthyl (**13f**), and 4-biphenyl group (**13g**) decreased the efficacy of the derivatives compared with **13a**. The introduction of a styryl group (**13h**) promoted antagonist activity ( $IC_{50} = 4.7 \pm 1.3 \mu M$ ,  $I_{max} = 66 \pm 2.3\%$ ) with no concomitant agonist activity. Finally, compound **13i** (MEKT-160) exhibited the most potent hPPAR $\gamma$  antagonist activity ( $IC_{50} = 0.17 \pm 0.02 \mu M$ ) in this series. We speculated that the rigid phenyl alkynyl moiety of **13i** might effectively interfere with the proper folding of H12, resulting in robust antagonist activity; however, this was a misunderstanding based on our X-ray crystallographic study as described later. Next, we attempted to modify the distal aromatic ring of **13i** to obtain potent PPAR $\gamma$  antagonists without any concomitant agonist activity. The SAR results indicated that the introduction of substituents at the 2-position of the distal benzene ring tended to diminish the PPAR $\gamma$  agonist activity. A 2-methyl derivative (**13j**) did not exhibit agonist activity although a 3-methyl derivative (**13k**) and 4-methyl derivative (**13l**) retained very low efficacy. Notably, 2-chloro or 2-bromo derivatives (**13m** and **13n**) had full antagonistic activity and blocked hPPAR $\gamma$  activation by 30  $\mu M$  pioglitazone completely with an  $IC_{50}$  value of 0.2–0.4  $\mu M$  without concomitant hPPAR $\gamma$  agonist activity. A 3-chlorophenyl derivative (**13o**) did not exhibit the same antagonist profile as **13m**. These results suggested that the appropriate steric bulkiness and proper substitution position of the halogen were necessary to obtain a full antagonist profile.

Next, we characterized the ligand-mediated cofactor recruitment elicited by the hPPAR $\gamma$  full agonist rosiglitazone (**1**) and hPPAR $\gamma$  antagonist MEKT-160 (**13i**) using a mammalian two-hybrid assay system [31]. Rosiglitazone (**1**) potently enhanced the positive interaction of the coactivator SMRT with hPPAR $\gamma$ ; however, no apparent interaction was detected for the hPPAR $\gamma$  antagonist MEKT-160 (Figure 8 left). Contrary to the coactivator recruitment, the corepressor NCoR–hPPAR $\gamma$  interaction was potently enhanced by MEKT-160 compared with rosiglitazone (Figure 8 right). Thus, the effects of MEKT-160 on cofactor recruitment to hPPAR $\gamma$  were markedly different from those of the hPPAR $\gamma$  agonist.



cpd.	R	PPAR $\gamma$ agonistic/antagonistic activity		
		EC <sub>50</sub> ( $\mu$ M) <sup>a</sup>	Emax (%) <sup>b</sup>	IC <sub>50</sub> ( $\mu$ M) <sup>c</sup>
pioglitazone		4.2	100	
MEKT-21		0.08	80	
13a	phenyl	0.29	19	N.T. <sup>f</sup>
13b	benzyl	0.71	65	
13c	2-phenylethyl	0.57	73	
13d	4-ethynylphenyl	0.29	19	N.T. <sup>f</sup>
13e	1-naphthyl	0.14	18	N.T. <sup>f</sup>
13f	2-naphthyl	0.04	16	N.T. <sup>f</sup>
13g	4-biphenyl	N.D. <sup>d</sup>	<10	>50
13h	styryl	ia. <sup>e</sup>	0	4.7 $\pm$ 1.3
13i (MMT-160)	phenylethynyl	N.D. <sup>d</sup>	<10	0.17 $\pm$ 0.02
13j	2Me-phenylethynyl	N.A. <sup>g</sup>	<10	0.63 $\pm$ 0.02
13k	3Me-phenylethynyl	N.D. <sup>d</sup>	0	0.41 $\pm$ 0.04
13l	4Me-phenylethynyl	N.D. <sup>d</sup>	<10	0.61 $\pm$ 0.05
13m	2Cl-phenylethynyl	N.A. <sup>g</sup>	0	0.28 $\pm$ 0.05
13n	2Br-phenylethynyl	N.A. <sup>g</sup>	0	0.63 $\pm$ 0.02
13o	3Cl-phenylethynyl	N.D. <sup>d</sup>	<10	0.62 $\pm$ 0.02
13p	2thienylethynyl	N.D. <sup>d</sup>	<10	0.37 $\pm$ 0.08
13q	1-naphthylethynyl	N.D. <sup>d</sup>	<10	>10
13r	2-naphthylethynyl	N.D. <sup>d</sup>	<10	>10

**Figure 7.** The PPAR $\gamma$  antagonistic activities of reversed amide derivatives. (a) Half maximal effective concentration. (b) Determined relative to the maximal activity of pioglitazone. (c) Concentration of test compound that afforded a 50% decrease in the maximal activity of pioglitazone (30  $\mu$ M). (d) Not determined. (e) Inactive at 10  $\mu$ M. (f) Not tested. (g) No activity at 30  $\mu$ M.

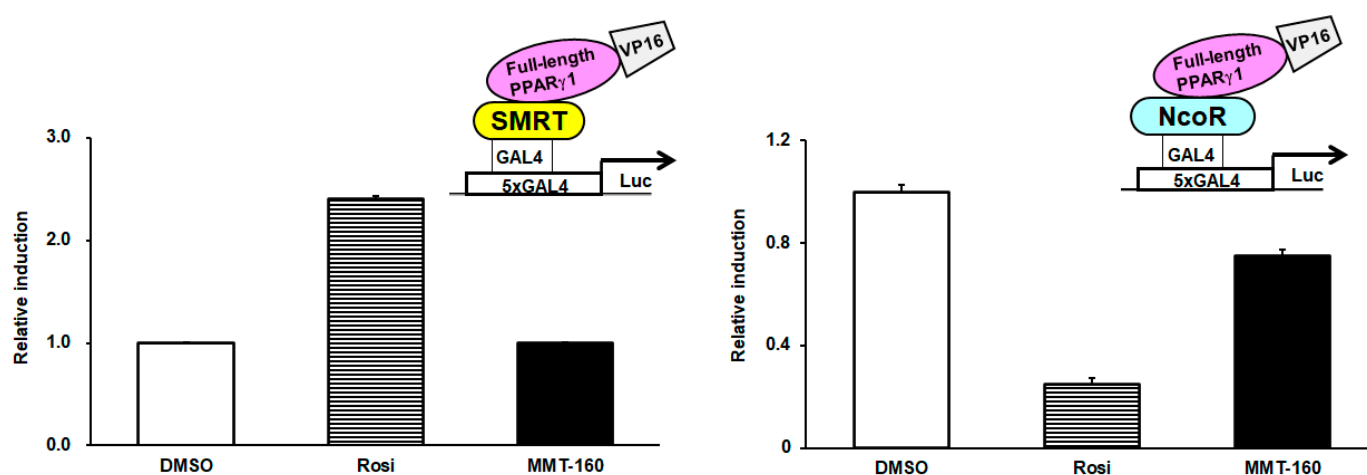


**Figure 8.** The functional analysis of the hPPAR $\gamma$  ligands using a mammalian two-hybrid assay. Data are presented as the fold induction relative to the DMSO control. Rosiglitazone (Rosi) was used at 30  $\mu$ M and MMT-160 was used at 10  $\mu$ M. All data points represent the average of triplicates ( $\pm$ SD). (Left) hPPAR $\gamma$ -SMRT two-hybrid assay with TK-MH100x4-LUC was performed in COS-1 cells. Transient transfection with VP16-PPAR $\gamma$  and Gal4-SMRT. (Right) hPPAR $\gamma$ -NCoR two-hybrid assay with TK-MH100x4-LUC was performed in COS-1 cells. Transient transfection with VP16-hPPAR $\gamma$  and Gal4-NCoR.

A previous study reported that PPAR $\gamma$ -corepressor association was involved in the development of obesity and diabetes [32,33]. Thus, compounds that regulate the corepressor

recruitment profile might be candidate agents for treating obesity and diabetes or useful biological tools to evaluate PPAR $\gamma$ -corepressor associations in biological models of obesity and diabetes.

hPPAR $\gamma$  is a well-known master regulator of adipogenesis; it promotes the conversion of a variety of preadipocytes and stem cell lines into mature adipocytes [34]. Thus, to characterize the effect of hPPAR $\gamma$  on adipocytes, we investigated the antagonistic activity of **13m** (a 2-chloro derivative of MEKT-160) on rosiglitazone-induced adipocyte differentiation. Preadipocyte 3T3-L1 cells were induced to differentiate by treatment with 1  $\mu$ M rosiglitazone and 5  $\mu$ g/mL insulin in the presence or absence of **13m**. As shown in Figure 9, rosiglitazone promoted adipocyte differentiation, as shown by an increase in the lipid content demonstrated by Oil red O staining. However, **13m** significantly inhibited rosiglitazone-induced adipocyte differentiation at 1  $\mu$ M, and completely suppressed it at 10  $\mu$ M. This result indicated that **13m** acts as a hPPAR $\gamma$  full antagonist at the cellular level.

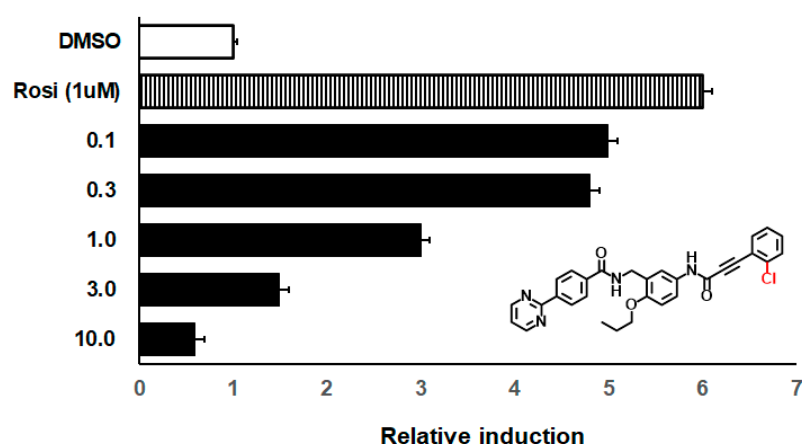


**Figure 9.** The effect of **13m** on the 1-induced adipogenesis of 3T3-L1 cells. After pretreatment with 1 (1 mM) and 5 mg/mL insulin, 3T3-L1 cells were incubated with the indicated concentrations of **13m**. Oil red O-stained cells are quantified at the bottom in terms of OD<sub>490</sub>. Data are presented as fold induction relative to the DMSO control. All data points represent the averages of triplicate samples ( $\pm$ SD).

#### 4. Arylalkynyl Amide-Type hPPAR $\gamma$ Antagonists Bind Covalently to hPPAR $\gamma$ via a Unique Binding Mode

Our structural development studies succeeded in creating the arylalkynyl amide-type hPPAR $\gamma$  antagonists such as MEKT-160 starting from the hPPAR $\gamma$  partial agonist, MEKT-21. We expected that the steric bulkiness and rigid arylalkynyl amide moiety of the compounds would interfere with the hPPAR $\gamma$  H12 and push the H12 out of the full agonist form position. To confirm this, an X-ray crystallographic structure analysis of the representative arylalkynyl amide-type hPPAR $\gamma$  antagonist complexed with the hPPAR $\gamma$  LBD could be performed. However, prior to that, we checked the chemical reactivity of arylalkynyl amides.

Arylalkynyl amides and esters are Michael acceptor structures, and various nucleophiles, such as sulfhydryl groups and amino groups, react with an alkynyl amide via Michael addition to form a nucleophile-substituted alkenyl amide (Michael adduct) [35,36]. Previously, oxidized unsaturated fatty acids and their derivatives, such as 4-oxodocosahexaenoic acid (4-oxoDHA), 6-oxooctadecatrienoic acid (6-oxo-OTE), and 15-deoxy-delta-12,14-prostaglandin J2 (15-dPGJ2), were reported to bind covalently to the Cys285 of the hPPAR $\gamma$  LBD [37,38]. In addition, the synthetic hPPAR $\gamma$  antagonists, GW9662 and T0070907 were shown to bind covalently to the Cys285 of the hPPAR $\gamma$  LBD [39,40]. These derivatives all contain a nucleophilic substitution spot. Considering this, we speculated that alkynyl amide-type hPPAR $\gamma$ -selective antagonists, such as MMT-160, might also bind covalently to the hPPAR $\gamma$  LBD, via the Cys285 in the H3 of the hPPAR $\gamma$  LBD. To confirm this, electrospray

ionization-mass spectrometry (ESI-MS) evaluation of the hPPAR $\gamma$  LBD after incubation with various ligands was performed (Figure 10) [41]. The apo form of the hPPAR $\gamma$  LBD had a molecular mass of 31,411 by ESI-MS, and in the presence of rosiglitazone or MEKT-21 (negative controls), the mass signal did not change. Conversely, in the presence of the covalent binder GW-9662, the mass signals shifted upward to a molecular mass that corresponded to the apo hPPAR $\gamma$  LBD + GW-9662 derivative. This clearly indicated that ESI-MS is useful to evaluate covalent binding. For MMT-160 and its 4-piperidine derivative, both of which contain an alkynyl amide structure, the mass signals were shifted upward to a higher molecular weight, with the molecular masses corresponding to the apo hPPAR $\gamma$  LBD + MMT-160 and apo hPPAR $\gamma$  LBD + 4-piperidine derivatives, respectively. Of note, a saturated carbonyl derivative of MMT-160 did not affect the mass signal of the apo form of the hPPAR $\gamma$  LBD.

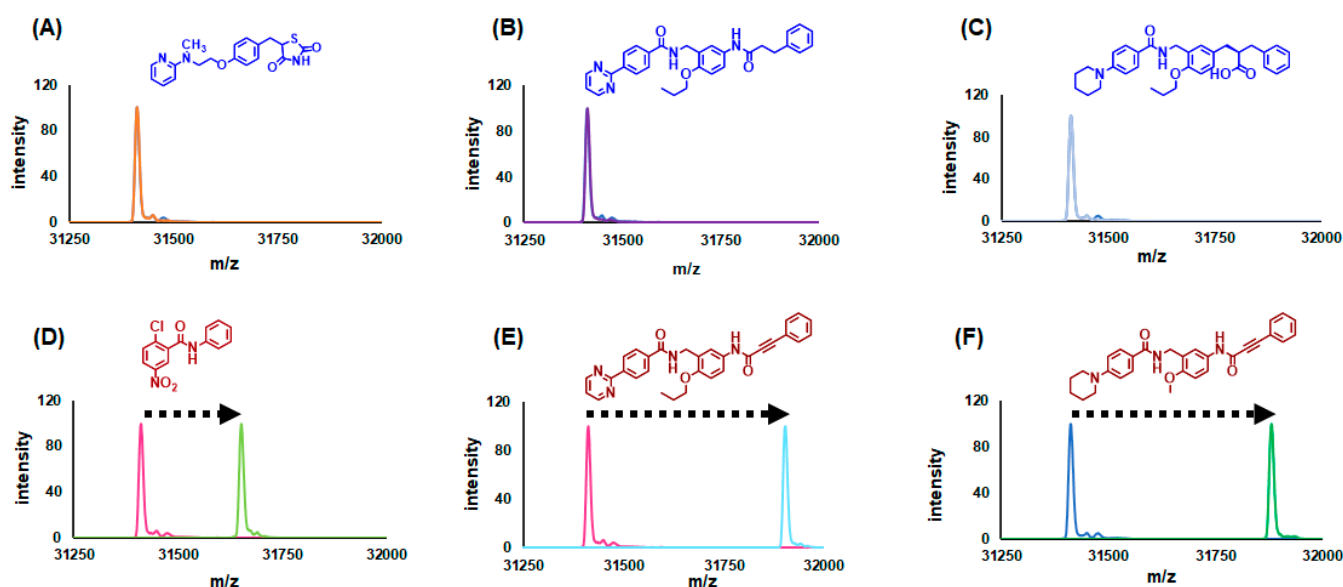


**Figure 10.** (A–F) ESI-MS spectrograms after the 24-h incubation of apo hPPAR $\gamma$  in the presence of various hPPAR $\gamma$  ligands. (A) Rosiglitazone (agonist). (B) **13m**. (C) MEKT-21. (D) GW-9662 (antagonist). (E) MMT-160. (F) MMT-160 derivative.

The ESI-MS analysis of the hPPAR $\gamma$  LBD after incubation with MMT-160 and its 4-piperidine derivative clearly indicated that these alkynyl amide derivatives bound covalently to the hPPAR $\gamma$  LBD.

To investigate the precise covalent binding mode of alkynyl arylamide-type hPPAR $\gamma$  antagonists further, we solved the X-ray crystallographic structure of MMT-160 complexed with the hPPAR $\gamma$  LBD homodimer at 3.0 Å resolution. A binary complex was obtained by co-crystallization (protein data bank accession code: 7WOX) (Figure 11A–E).

Only one hPPAR $\gamma$  LBD in the homodimer (designated as chain A) was able to be refined in the structure of MMT-160 (Figure 11A). The phenyl acetylenyl (Michael acceptor) portion of MMT-160 was docked in the Y1 arm of the binding pocket extending through the space between the helices, H3, H4, and H12, and formed hydrophobic interactions (Figure 11B). Distinct electron density was observed around the sulfhydryl group of Cys285 and the distance between the sulfhydryl group of Cys285 and the benzylic carbon of MMT-160 was estimated as 1.80 Å, consistent with the theoretical C–S bond length (Figure 11B). No apparent hydrogen bond interactions were observed between MMT-160 and five critical amino acids: Ser289, His323, Tyr327, His449, and especially Tyr473. The lack of these interactions might explain why MMT-160 did not exhibit obvious hPPAR $\gamma$  agonistic activity (Figure 11B).

Surprisingly, the two other hydrophobic side chains of MMT-160 were found to dock into the unexpected binding sites. The *n*-propoxy side chain hosted in the Y2 arm, situated

between H3 and the  $\beta$ -sheet, also formed hydrophobic interactions (Figure 11C). What was most surprising was that the pyrimidine-2-yl benzamide of MMT-160 was not buried in the large binding pocket of the hPPAR $\gamma$  LBD but extended out from the pocket and the carbonyl oxygen formed hydrogen bond interactions with Gly284 (Figure 11D). These data indicated that MMT-160 was docked into to the hPPAR $\gamma$  LBD—mainly via hydrophobic interactions with the Y1- and Y2-arm amino acids—in addition to its covalent binding to CYS285.

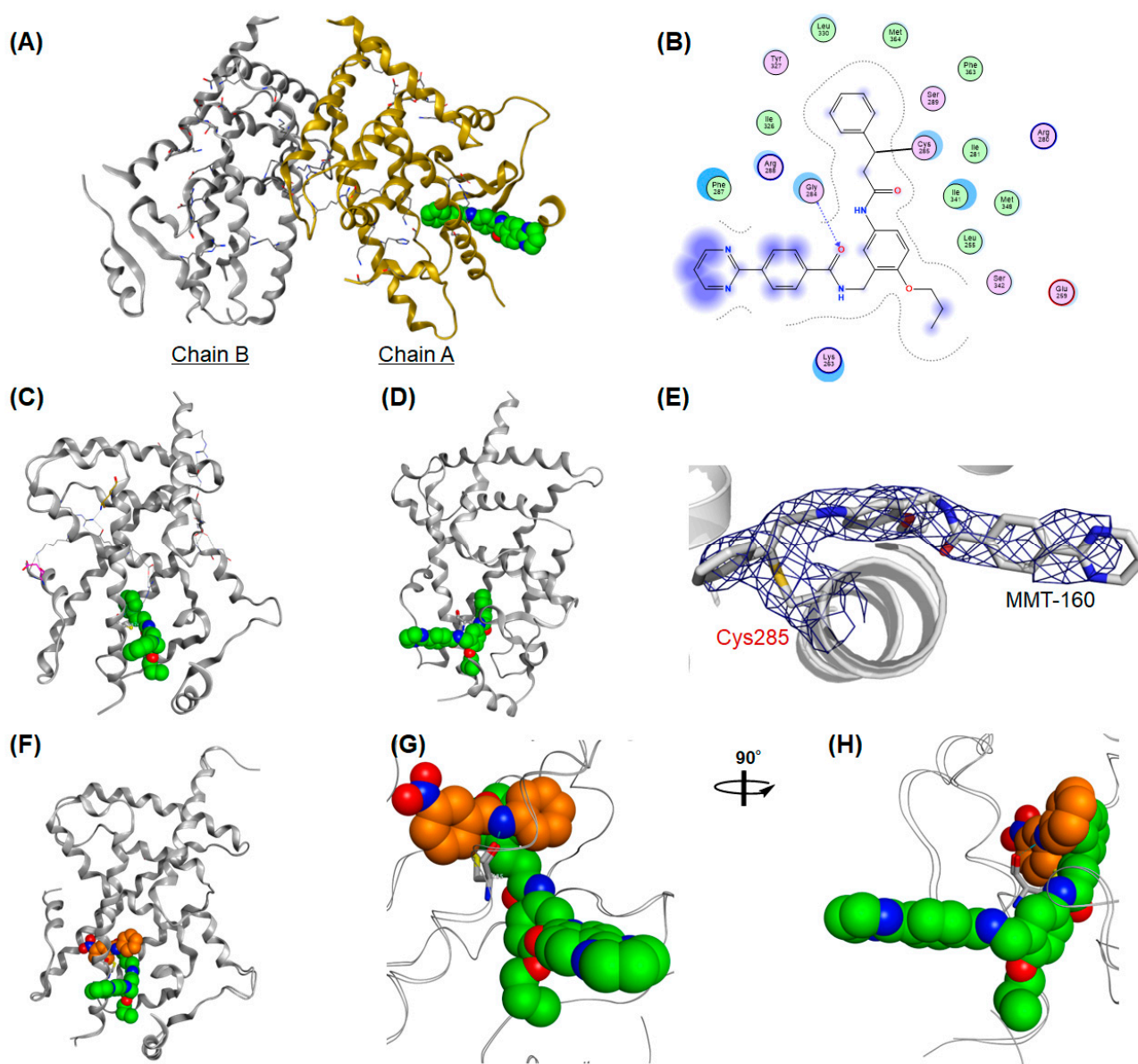


**Figure 11.** The binding mode of MMT-160 complexed with the hPPAR $\gamma$  LBD. (A) Whole structure of the hPPAR $\gamma$  LBD–MMT-150 homodimer (PDB: 7WOX). Proteins are represented as a gray and a yellow ribbon model and MMT-150 is depicted as a green van der Waals model. (B) Two-dimensional interaction map of the hPPAR $\gamma$  LBD and MMT-150. (C,D) Whole structure of the non-full agonist form of hPPAR $\gamma$  LBD–MMT-160. Proteins are represented as a van der Waals surface model and MMT-160 is depicted as a green van der Waals model. (D) Zoomed-in view of the covalent binding mode of MMT-160 to CYS285. (E–H) Superimposed structures of GW-9662 and MMT-160 docked into the hPPAR $\gamma$  LBD. Proteins are represented as ribbon and wire models. GW-9662 is depicted as a brown van der Waals model and MMT-160 is depicted as a green van der Waals model.

As described previously, the entrance to the ligand binding site of the hPPAR $\gamma$  LBD was reported to be between H3 and a three-stranded antiparallel  $\beta$ -sheet. We focused our attention on the entrance site. Figure 11F–H clearly shows that MMT-160 covalently bound to CYS285 on the H3 shielded the entrance site of the ligand more effectively than GW-9662.

We found that the arylalkynyl amide-type hPPAR $\gamma$  antagonists bound covalently to the CYS285 of the PPAR $\gamma$  LBD via Michael addition. The X-ray crystallographic analysis of the hPPAR $\gamma$  LBD complexed with MMT-160 indicated its unique binding mode, which is quite different from the recently reported PPAR $\gamma$  antagonists of SR-10171 (phenoxyacetic acid derivative) and SR-11023 (phenylacetic acid derivative) [42], thus supporting some of the antagonistic nature of MMT-160.

## 5. Conclusions

Two types of hPPAR $\gamma$  antagonists: a non-covalently bound antagonist, MEKT-76, and a covalently bound antagonist, MMT-160, were created. Generally, when the allosteric binding site occupancy ratio with the ligand increased, the ligand tended to show a greater antagonistic effect (Figure 12).

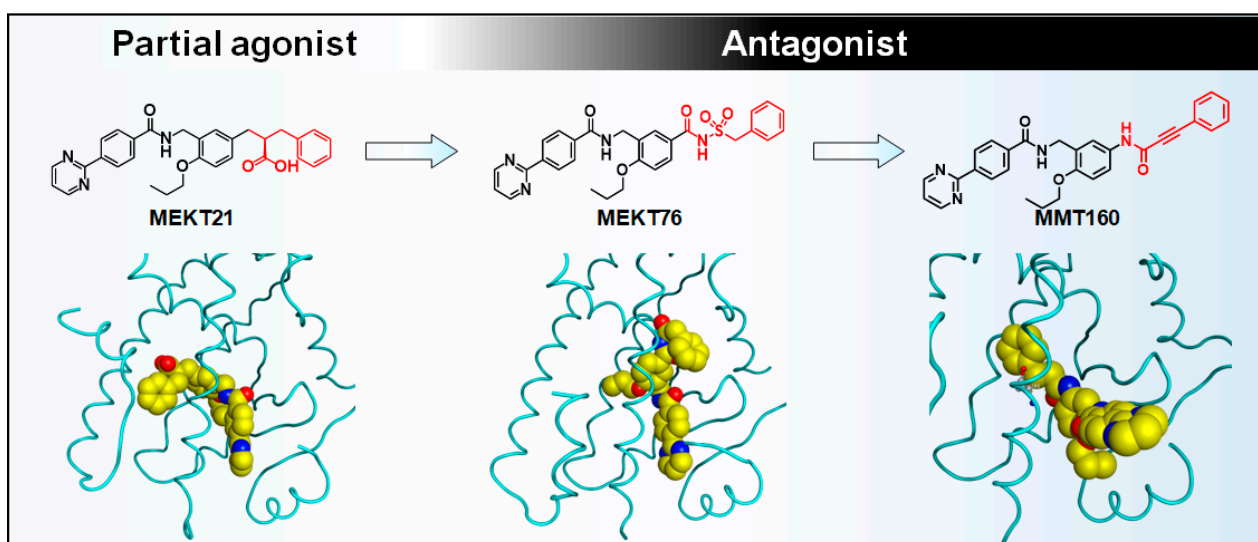


**Figure 12.** The structural development of an hPPAR $\gamma$  antagonist from an hPPAR $\gamma$  agonist. The structures and binding modes of MEKT-21, MEKT-75, and MMT-160 are depicted.

Both series of compounds were structurally derived from our original hPPAR $\gamma$  agonist, MEKT-21.

Our study demonstrated that the agonist–antagonist switching concept—a simple medicinal chemistry strategy for the design of nuclear receptor antagonists—can be used to develop hPPAR $\gamma$  antagonists. This strategy is also applicable to create other nuclear receptor antagonists [43,44]. However, we speculated that our strategy created folding inhibition-type antagonists of hPPAR $\gamma$ , which have no direct hydrogen bond interactions with the Tyr473 of H12, resulting in pushing the H12 out of position. Is our speculation correct? The answer is “not yet!”

A recent X-ray crystallographic study of the hPPAR $\gamma$  ligands SR-10171 (inverse agonist) and SR-11023 (antagonist) complexed with the hPPAR $\gamma$  LBD confirmed our speculation/working hypothesis. These compounds are thought to be H12 folding inhibition-type antagonists of hPPAR $\gamma$ . Both ligands are docked between the H3 and  $\beta$ -sheet of the hPPAR $\gamma$  LBD and wrap around the solvent-exposed face of H3. Importantly, the hydrophobic tails of SR10171 and SR11023 form hydrophobic interactions between the H3 and H12 of the hPPAR $\gamma$  LBD and stabilize H12 at H3, away from the AF2 coactivator-binding surface.

On the basis of this, our next idea (plan C) involves the introduction/replacement of other hydrophobic substituents at the proper position of MMT-160, which will interact

hydrophobically with the H12 of the hPPAR $\gamma$  LBD and pull the H12 to a position near to the newly introduced/replaced hydrophobic substituents. We expect that the hot spot should be an *n*-propoxy group and/or 4-(pyrimidin-2-yl)benzamide moiety of MMT-160. We are now conducting further structural studies related to the development of covalent-binding hPPAR $\gamma$  ligands.

**Funding:** This work was supported by the Targeted Proteins Research Program of the Japan Science and Technology Corporation, the Platform for Drug Discovery, Informatics, and Structural Life Science from the Ministry of Education, Culture, Sports, Science and Technology, Japan, and a Grant in-aid for Scientific Research KAKENHI (B) (grant number 26293027 to H.M.) from the Ministry of Education, Culture, Sports, Science and Technology, Japan.

**Institutional Review Board Statement:** Not applicable.

**Informed Consent Statement:** Not applicable.

**Data Availability Statement:** Data sharing not applicable.

**Acknowledgments:** The author gives special thanks to Masao Ohashi (Okayama University, Japan) for the synthesis and evaluation of many PPAR ligands, Takuji Ohyama (Yamanashi University, Japan), and Toshimasa Ito (Showa-Yakka University, Japan) for their X-ray crystallographic studies. The author thanks all collaborators who contributed to our published body of work.

**Conflicts of Interest:** The author declares no conflict of interest.

### Abbreviations

PPAR	peroxisome proliferator-activated receptor
H12	helix 12
LBD	ligand binding domain
NR	nuclear receptor
DNA	deoxyribonucleic acid
PPRE	peroxisome proliferator responsive element
DR1	hexameric AGGTCA recognition motif, separated by one nucleotide
AF-1	transactivation function-1
AF-2	transcriptional activation function-2
TZD	thiazolidinedione-2:4-dione
Cdk5	cyclin-dependent kinase 5
LBP	ligand-binding pocket
Ser	serine
His	histidine
Tyr	tyrosine
DEPC	diethyl cyanophosphonate
EDC	1-(3-dimethylaminopropyl)-3-ethylcarbodiimide hydrochloride
DMAP	4-dimethylaminopyridine
vdW	van der Waals
SAR	Structure-Activity Relationship
DRIP205	vitamin D-interacting protein 205
NCoR	nuclear receptor corepressor
oxoDHA	oxo docosahexaenoic acid
oxo-OE	oxo octadecatrienoic acid
dPGJ2	deoxy-delta-12:14-prostaglandin J2
Cys	cysteine
ESI-MS	electrospray ionization-mass spectrometry
Gly	glycine

## References and Note

1. Scholtes, C.; Giguère, V. Transcriptional control of energy metabolism by nuclear receptors. *Nat. Rev. Mol. Cell Biol.* **2022**, *23*, 750–770. [[CrossRef](#)] [[PubMed](#)]
2. Montaigne, D.; Butruille, L.; Staels, B. PPAR control of metabolism and cardiovascular functions. *Nat. Rev. Cardiol.* **2021**, *18*, 809–823. [[CrossRef](#)] [[PubMed](#)]
3. Tahri-Joutey, M.; Andreoletti, P.; Surapureddi, S.; Nasser, B.; Cherkaoui-Malki, M.; Latruffe, N. Mechanisms Mediating the Regulation of Peroxisomal Fatty Acid Beta-Oxidation by PPAR $\alpha$ . *Int. J. Mol. Sci.* **2021**, *22*, 8969. [[CrossRef](#)] [[PubMed](#)]
4. Bervejillo, M.L.; Ferreira, A.M. Understanding Peroxisome Proliferator-Activated Receptors: From the Structure to the Regulatory Actions on Metabolism. *Adv. Exp. Med. Biol.* **2019**, *1127*, 39–57. [[CrossRef](#)]
5. Christofides, A.; Konstantinidou, E.; Jani, C.; Boussiotis, V.A. The role of peroxisome proliferator-activated receptors (PPAR) in immune responses. *Metabolism* **2020**, *114*, 154338. [[CrossRef](#)]
6. Lee, J.-E.; Schmidt, H.; Lai, B.; Ge, K. Transcriptional and Epigenomic Regulation of Adipogenesis. *Mol. Cell Biol.* **2019**, *39*, e00601–e00618. [[CrossRef](#)]
7. Kökény, G.; Calvier, L.; Hansmann, G. PPAR $\gamma$  and TGF $\beta$ -major regulators of metabolism, inflammation, and fibrosis in the lungs and kidneys. *Int. J. Mol. Sci.* **2021**, *22*, 10431. [[CrossRef](#)]
8. Tontonoz, P.; Spiegelman, B.M. Fat and beyond: The diverse biology of PPAR $\gamma$ . *Annu. Rev. Biochem.* **2008**, *77*, 289–312. [[CrossRef](#)]
9. Kawai, M.; Rosen, C.J. PPAR $\gamma$ : A circadian transcription factor in adipogenesis and osteogenesis. *Nat. Rev. Endocrinol.* **2010**, *6*, 629–636. [[CrossRef](#)]
10. Alhowail, A.; Alsikhan, R.; Alsaud, M.; Aldubayan, M.; Rabbani, S.I. Protective Effects of Pioglitazone on Cognitive Impairment and the Underlying Mechanisms: A Review of Literature. *Drug Des. Dev. Ther.* **2022**, *16*, 2919–2931. [[CrossRef](#)]
11. Whitehead, J.P. Diabetes: New conductors for the peroxisome proliferator-activated receptor  $\gamma$  (PPAR $\gamma$ ) orchestra. *Int. J. Biochem. Cell Biol.* **2011**, *43*, 1071–1074. [[CrossRef](#)] [[PubMed](#)]
12. Shang, J.; Brust, R.; Mosure, S.A.; Bass, J.; Munoz-Tello, P.; Lin, H.; Hughes, T.S.; Tang, M.; Ge, Q.; Kamenekca, T.M.; et al. Cooperative cobinding of synthetic and natural ligands to the nuclear receptor PPAR $\gamma$ . *Elife* **2018**, *7*, e43320. [[CrossRef](#)] [[PubMed](#)]
13. Silvestro, S.; Schepici, G.; Bramanti, P.; Mazzon, E. Molecular Targets of Cannabidiol in Experimental Models of Neurological Disease. *Molecules* **2020**, *25*, 5186. [[CrossRef](#)]
14. Stark, J.M.; Coquet, J.M.; Tibbitt, C.A. The Role of PPAR- $\gamma$  in Allergic Disease. *Curr. Allergy Asthma Rep.* **2021**, *21*, 45. [[CrossRef](#)]
15. Lefere, S.; Puengel, T.; Hundertmark, J.; Penners, C.; Frank, A.K.; Guillot, A.; de Muyneck, K.; Heymann, F.; Adarbes, V.; Defrène, E.; et al. Differential effects of selective- and pan-PPAR agonists on experimental steatohepatitis and hepatic macrophages. *J. Hepatol.* **2020**, *3*, 757–770. [[CrossRef](#)] [[PubMed](#)]
16. Miyachi, H. Structural biology-based exploration of subtype-selective agonists for peroxisome proliferator-activated receptors. *Int. J. Mol. Sci.* **2021**, *22*, 9223. [[CrossRef](#)] [[PubMed](#)]
17. Hashimoto, Y.; Miyachi, H. Nuclear receptor antagonists designed based on the helix-folding inhibition hypothesis. *Bioorganic Med. Chem.* **2005**, *13*, 5080–5093. [[CrossRef](#)]
18. Ban, S.; Ueda, Y.; Ohashi, M.; Matsuno, K.; Ikeda, M.; Kato, N.; Miyachi, H. Peroxisome proliferator-activated receptor delta antagonists inhibit hepatitis C virus RNA replication. *Bioorganic Med. Chem. Lett.* **2013**, *23*, 4774–4778. [[CrossRef](#)]
19. Asano, L.; Ito, I.; Kuwabara, N.; Waku, T.; Yanagisawa, J.; Miyachi, H.; Shimizu, T. Structural basis for vitamin D receptor agonism by novel non-secosteroidal ligands. *FEBS Lett.* **2013**, *587*, 957–963. [[CrossRef](#)]
20. Aoyama, A.; Endo-Umeda, K.; Kishida, K.; Ohgane, K.; Noguchi-Yachide, T.; Aoyama, H.; Ishikawa, M.; Miyachi, H.; Makishima, M.; Hashimoto, Y. Design, synthesis, and biological evaluation of novel transrepression-selective liver X receptor (LXR) ligands with 5,11-dihydro-5-methyl-11-methylene-6H-dibenz[b,e]azepin-6-one skeleton. *J. Med. Chem.* **2012**, *55*, 7360–7377. [[CrossRef](#)]
21. Ohashi, M.; Oyama, T.; Putranto, E.W.; Waku, T.; Nobusada, H.; Kataoka, K.; Matsuno, K.; Yashiro, M.; Morikawa, K.; Huh, N.-H.; et al. Design and synthesis of a series of  $\alpha$ -benzyl phenylpropanoic acid-type peroxisome proliferator-activated receptor (PPAR) gamma partial agonists with improved aqueous solubility. *Bioorganic Med. Chem.* **2013**, *21*, 2319–2332. [[CrossRef](#)] [[PubMed](#)]
22. Einstein, M.; Akiyama, T.E.; Castriota, G.A.; Wang, C.F.; McKeever, B.; Mosley, R.T.; Becker, J.W.; Moller, D.E.; Meinke, P.T.; Wood, H.B.; et al. The Differential Interactions of Peroxisome Proliferator-Activated Receptor  $\gamma$  Ligands with Tyr473 Is a Physical Basis for Their Unique Biological Activities. *Mol. Pharmacol.* **2008**, *73*, 62–74. [[CrossRef](#)] [[PubMed](#)]
23. Ohashi, M.; Gamo, K.; Oyama, T.; Miyachi, H. Peroxisome proliferator-activated receptor gamma (PPAR $\gamma$ ) has multiple binding points that accommodate ligands in various conformations: Structurally similar PPAR $\gamma$  partial agonists bind to PPAR $\gamma$  LBD in different conformations. *Bioorganic Med. Chem. Lett.* **2015**, *25*, 2758–2762. [[CrossRef](#)]
24. Ohashi, M.; Oyama, T.; Miyachi, H. Different structures of the two peroxisome proliferator-activated receptor gamma (PPAR $\gamma$ ) ligand-binding domains in homodimeric complex with partial agonist, but not full agonist. *Bioorganic Med. Chem. Lett.* **2015**, *25*, 2639–2644. [[CrossRef](#)] [[PubMed](#)]
25. Nolte, R.T.; Wisely, G.B.; Westin, S.; Cobb, J.E.; Lambert, M.H.; Kurokawa, R.; Rosenfeld, M.G.; Willson, T.M.; Glass, C.K.; Milburn, M.V. Ligand binding and co-activator assembly of the peroxisome proliferator-activated receptor-gamma. *Nature* **1998**, *395*, 137–143. [[CrossRef](#)]
26. The total interaction energy calculation was performed with MOE (Molecular Operating Environment, ver. 2020.09)

27. Hughes, T.; Chalmers, M.J.; Novick, S.; Kuruvilla, D.S.; Chang, M.R.; Kamenecka, T.M.; Rance, M.; Johnson, B.A.; Burris, T.; Griffin, P.R.; et al. Ligand and Receptor Dynamics Contribute to the Mechanism of Graded PPAR $\gamma$  Agonism. *Structure* **2012**, *20*, 139–150. [[CrossRef](#)]
28. Shang, J.; Kojetin, D.J. Structural mechanism underlying ligand binding and activation of PPAR $\gamma$ . *Structure* **2021**, *29*, 940–950.e4. [[CrossRef](#)]
29. Ohashi, M.; Miyachi, H. Design and Synthesis of Peroxisome Proliferator-activated Receptor (PPAR) Gamma Antagonists Based on the Principle of Operation of Nuclear Receptor I. *Yakugaku Zasshi* **2017**, *137*, 957–967. [[CrossRef](#)]
30. Daniel, D.; Andrew, A.S. Reductive N-alkylation of amides, carbamates and ureas. *Tetrahedron Lett.* **1999**, *40*, 2295–2298.
31. Adachi, R.; Shulman, A.I.; Yamamoto, K.; Shimomura, I.; Yamada, S.; Mangelsdorf, D.J.; Makishima, M. Structural Determinants for Vitamin D Receptor Response to Endocrine and Xenobiotic Signals. *Mol. Endocrinol.* **2004**, *18*, 43–52. [[CrossRef](#)]
32. Cohen, R.N. Nuclear receptor corepressors and PPAR. *Nucl. Recept. Signal.* **2006**, *4*, e003. [[CrossRef](#)] [[PubMed](#)]
33. Li, P.; Fan, W.; Xu, J.; Lu, M.; Yamamoto, H.; Auwerx, J.; Sears, D.D.; Talukdar, S.; Oh, D.; Chen, A.; et al. Adipocyte NCoR knockout decreases PPAR $\gamma$  phosphorylation and enhances PPAR $\gamma$  activity and insulin sensitivity. *Cell* **2011**, *147*, 815–826. [[CrossRef](#)] [[PubMed](#)]
34. Shao, X.; Wang, M.; Wei, X.; Deng, S.; Fu, N.; Peng, Q.; Jiang, Y.; Ye, L.; Xie, J.; Lin, Y. Peroxisome proliferator-activated re-ceptor- $\gamma$ : Master regulator of adipogenesis and obesity. *Curr. Stem. Cell Res. Ther.* **2016**, *11*, 282–289. [[CrossRef](#)] [[PubMed](#)]
35. Gorsuch, S.; Bavetsias, V.; Rowlands, M.G.; Aherne, W.; Workman, P.; Jarman, M.; McDonald, E. Synthesis of isothiazol-3-one derivatives as inhibitors of histone acetyltransferases (HATs). *Bioorganic Med. Chem.* **2009**, *17*, 467–474. [[CrossRef](#)]
36. Kojima, H.; Fujita, Y.; Takeuchi, R.; Ikebe, Y.; Ohashi, N.; Yamamoto, K.; Itoh, T. Cyclization Reaction-Based Turn-on Probe for Covalent Labeling of Target Proteins. *Cell Chem. Biol.* **2020**, *27*, 334–349.e11. [[CrossRef](#)]
37. Itoh, T.; Fairall, L.; Amin, K.; Inaba, Y.; Szanto, A.; Balint, B.L.; Nagy, L.; Yamamoto, K.; Schwabe, J.W. Structural basis for the activation of PPAR $\gamma$  by oxidized fatty acids. *Nat. Struct. Mol. Biol.* **2008**, *15*, 924–931. [[CrossRef](#)]
38. Shiraki, T.; Kamiya, N.; Shiki, S.; Kodama, T.S.; Kakizuka, A.; Jingami, H. Alpha, beta-unsaturated ketone is a core moiety of natural ligands for covalent binding to peroxisome proliferator-activated receptor gamma. *J. Biol. Chem.* **2005**, *280*, 14145–14153. [[CrossRef](#)]
39. Zhou, Y.; Guo, T.; Tang, G.; Wu, H.; Wong, N.-K.; Pan, Z. Site-Selective Protein Immobilization by Covalent Modification of GST Fusion Proteins. *Bioconjugate Chem.* **2014**, *25*, 1911–1915. [[CrossRef](#)]
40. Lee, G.; Elwood, F.; McNally, J.; Weiszmann, J.; Lindstrom, M.; Amaral, K.; Nakamura, M.; Miao, S.; Cao, P.; Learned, R.M.; et al. T0070907, a selective ligand for peroxisome proliferator-activated receptor gamma, functions as an antagonist of biochemical and cellular activities. *J. Biol. Chem.* **2002**, *277*, 19649–19657. [[CrossRef](#)]
41. Yoshizawa, M.; Aoyama, T.; Itoh, T.; Miyachi, H. Arylalkynyl amide-type peroxisome proliferator-activated receptor  $\gamma$  (PPAR $\gamma$ )-selective antagonists covalently bind to the PPAR $\gamma$  ligand binding domain with a unique binding mode. *Bioorganic Med. Chem. Lett.* **2022**, *64*, 128676. [[CrossRef](#)]
42. Frkic, R.L.; Marshall, A.; Blayo, A.-L.; Pukala, T.; Kamenecka, T.M.; Griffin, P.R.; Bruning, J.B. PPAR $\gamma$  in Complex with an Antagonist and Inverse Agonist: A Tumble and Trap Mechanism of the Activation Helix. *Iscience* **2018**, *5*, 69–79. [[CrossRef](#)] [[PubMed](#)]
43. Mori, S.; Tsuemoto, N.; Kasagawa, T.; Nakano, E.; Fujii, S.; Kagechika, H. Development of Boron-Cluster-Based Progesterone Receptor Antagonists Bearing a Pentafluorosulfanyl (SF<sub>5</sub>) Group. *Chem. Pharm. Bull.* **2019**, *67*, 1278–1283. [[CrossRef](#)] [[PubMed](#)]
44. Kaitoh, K.; Nakatsu, A.; Mori, S.; Kagechika, H.; Hashimoto, Y.; Fujii, S. Design, Synthesis and Biological Evaluation of Novel Nonsteroidal Progesterone Receptor Antagonists Based on Phenylamino-1,3,5-triazine Scaffold. *Chem. Pharm. Bull.* **2019**, *67*, 566–575. [[CrossRef](#)] [[PubMed](#)]

**Disclaimer/Publisher’s Note:** The statements, opinions and data contained in all publications are solely those of the individual author(s) and contributor(s) and not of MDPI and/or the editor(s). MDPI and/or the editor(s) disclaim responsibility for any injury to people or property resulting from any ideas, methods, instructions or products referred to in the content.